Available online at www.sciencedirect.com
SCIENCE DIRECT®
International Journal of Multiphase Flow 31 (2005) 1220–1230
International Journal of Multiphase Flow
www.elsevier.com/locate/ijmulflow

Brief communication

Preferential concentration of particles in homogeneous and isotropic turbulence

A.M. Wood, W. Hwang *, J.K. Eaton

Department of Mechanical Engineering, Stanford University, 488 Escondido Mall, Building 500, Stanford, CA 94305-3035, USA

Received 10 February 2005; received in revised form 10 July 2005

Keywords: Particle dispersion; Preferential concentration; Homogeneous isotropic turbulence

1. Introduction

Non-homogeneous particle concentrations resulting from the carrier fluid turbulence occur frequently in nature as well as in many industrial processes. For this reason, it is important to fully understand the mechanisms that lead to this occurrence in order to use them advantageously. Many experiments and numerical simulations have been conducted to explore this phenomenon, known as preferential concentration. Maxey (1987), Squires and Eaton (1991), and Fessler et al. (1994) have shown that particles subjected to specific turbulent conditions tend to concentrate non-uniformly into areas of low vorticity and high strain rate.

The major parameter determining the degree of preferential concentration is the Stokes number, defined in Eq. (1.1).

$$St \equiv \frac{\tau_p}{\tau_f} \tag{1.1}$$

Here, τ_p is the aerodynamic time constant of the particle, and τ_f is an appropriate fluid time scale. Many previous workers (e.g. see Wang and Maxey, 1993; Fallon and Rogers, 2002) have used the

* Corresponding author. Present address: Engine Combustion Department, Combustion Research Facility, Sandia National Laboratories, P.O. Box 969, MS 9053, Livermore, CA 94551, USA. Tel.: +1 925 294 6092; fax: +1 925 294 1004.

E-mail address: wthwang@stanfordalumni.org (W. Hwang).

0301-9322/$ - see front matter
doi:10.1016/j.ijmultiphaseflow.2005.07.001

Kolmogorov time scale, τ_k, as the fluid time scale because it is the scale on which the highest vorticity gradients occur. Previous work has shown that the peak in preferential concentration occurs for Stokes number near one using this fluid time scale. As the ratio of τ_p/τ_k approaches zero, the particles start resembling fluid elements and tend to follow streamlines exactly, resulting in a uniform distribution of particles. As τ_p/τ_k increases to values much greater than one, the particles tend to follow ballistic trajectories and are only influenced by the largest, most energetic eddies. Therefore, high Stokes number particles are also uniformly distributed (being dispersed by turbulent diffusion). In the special case where the Stokes number is near one, inertia prevents the particles from following vortex streamlines precisely and results in particles being centrifuged away from vortex cores, thus preferentially concentrating in areas of low vorticity and high strain rate. Most of the previous work performed in near homogeneous and isotropic turbulence has been conducted at low turbulent Reynolds numbers where the turbulence has a relatively narrow range of scales. Therefore it is not certain that the Kolmogorov scale is the correct fluid time scale or how sharp the peak may be in preferential concentration as a function of Stokes number.

In recent numerical studies, Hogan and Cuzzi (2001) examined preferential concentration for Taylor Reynolds numbers from 40 to 140 and concluded that preferential concentration is maximized at Kolmogorov Stokes numbers near one. They expect this trend to continue for even higher Reynolds numbers. However, it is difficult to test this hypothesis because of the extensive computing resources required.

The objective of this work was to extend the range of Reynolds numbers for preferential concentration studies by using an experimental apparatus to produce homogeneous isotropic particle-laden turbulence at Reynolds numbers beyond that achieved in previous numerical and experimental work. We also compare two different descriptors of preferential concentration to assess their consistency, and examine the length scales that correspond to preferential concentration.

2. Experimental facility

Experiments were conducted in the approximately internally spherical turbulence chamber described by Hwang and Eaton (2004). Eight synthetic jet actuators aimed at the center of the chamber act to create homogeneous and isotropic turbulence with no mean flow (see Fig. 1). The speakers used to create the jets are driven by random sine waves, with the turbulence intensity controlled by an eight-channel digital amplifier. Qualification experiments reported in Hwang and Eaton (2004) prove that the turbulence is highly isotropic and homogeneous in the central region of the chamber. Spatial maps of the horizontal-to-vertical root mean square (rms) velocity ratio show isotropy, with values centered at 1.0 and varying less than $\pm 20\%$ over the 40 mm $\times$ 40 mm domain. Similarly, the turbulence kinetic energy normalized by its spatial average fluctuates within $\pm 10\%$ over the same domain, indicating homogeneity.

Three classes of particles were tested in this experiment. The inertia of the particles can be represented by the particle time constant, τ_p. Eq. (2.1) defines τ_p in the limit of creeping flow, where ρ_p is the particle density, d_p is the particle diameter, and μ is the dynamic viscosity of the fluid.

$$\tau_p = \frac{\rho_p d_p^2}{18\mu} \tag{2.1}$$

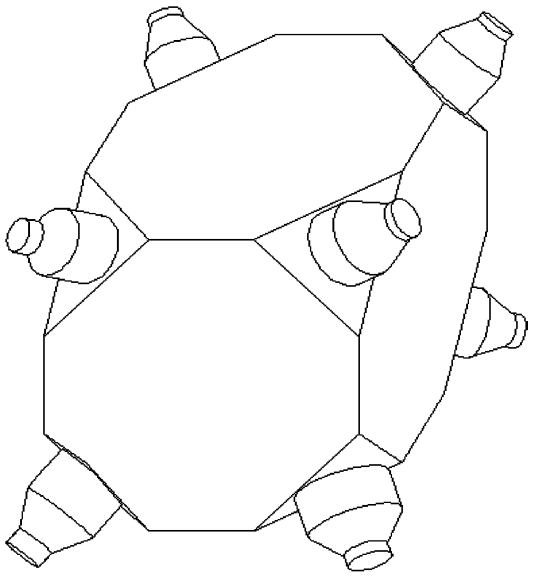

Fig. 1. Turbulence chamber.

Lycopodium particles with a density of 700 kg/m^3 and a nominal diameter of 25 μm, as well as two sets of glass particles, both with a density of 2450 kg/m^3, with nominal diameters of 20 and 50 μm, were used. For particle Reynolds number, Re_p, greater than 0.01, the equation for τ_p is corrected by the factor shown in Eq. (2.2).

$$\tau_p = \frac{\rho_p d_p^2}{18\mu} \frac{1}{1 + 0.15 Re_p^{0.687}} \tag{2.2}$$

This equation was derived by assuming a steady mean flow (slip velocity) around the particle. For this experiment, there was no mean flow, and the particles had not reached their terminal velocities (which were much less than the fluid turbulent fluctuations) inside the chamber. The turbulent rms velocity, u_{rms}, could therefore be thought of as the "effective" velocity that the particle sees, and was used to calculate Re_p. The particle Reynolds number was approximately 1.0, 0.9, and 2.2 for the lycopodium, 20 μm glass, and 50 μm glass particles, respectively, resulting in particle time constants ranging from 1 to 15 ms, as listed in Table 1. The nominal diameter and size distribution of the particles were verified by measurements using a Coulter Counter. Both sizes of glass particles were tested under two different turbulence settings corresponding to different turbulence intensities and Kolmogorov time scales, shifting the Stokes number slightly. The two turbulence conditions had a Taylor microscale Reynolds number, Re_λ, near 230. Experimental properties are listed in Tables 1 and 2.

Particles were placed initially in the sealed end of a bent over flexible tube, with the other end connected to the top of the turbulence chamber. The particles were gravity-fed into the chamber by inverting the particle-filled flexible tube connected to the top of the chamber, and dispersed by a screen as they entered the chamber as shown in Fig. 2. When the particles were first dropped into the chamber, a thick plume saturated the image followed by a gradual settling of the particles,

Table 1
Particle properties

	Material	Lycopodium	Glass	Glass
d_p	Nominal diameter (μm)	25	20	50
$\overline{d_p}$	Measured mean diameter (μm)	24.4	19.8	51.5
σ_p	Standard deviation of diameter (μm)	1.4	4.4	3.8
ρ_p	Density (kg/m^3)	700	2450	2450
τ_p	Particle time constant (ms) at $q^2 = 1.1$ m^2/s^2	1.09	2.55	15.63
τ_p	Particle time constant (ms) at $q^2 = 1.4$ m^2/s^2	1.08	2.53	15.39
St_k	Stokes number at $q^2 = 1.1$ m^2/s^2		1.06	6.51
St_k	Stokes number at $q^2 = 1.4$ m^2/s^2	0.57	1.33	8.10

Table 2
Turbulence settings

U_1	Mean velocity (horizontal) (m/s)	0.0799	0.0624
U_2	Mean velocity (vertical) (m/s)	0.0880	0.1933
$u_{1,rms}$	Root mean square velocity (horizontal) (m/s)	0.620	0.689
$u_{2,rms}$	Root mean square velocity (vertical) (m/s)	0.600	0.677
q^2	Twice the turbulence kinetic energy (m^2/s^2)	1.1	1.4
τ_k	Kolmogorov time scale (ms)	2.4	1.9
η	Kolmogorov length scale (mm)	0.19	0.17
λ	Taylor microscale (mm)	5.6	5.1
Re_λ	Taylor microscale Reynolds number	228	233
ε	Viscous dissipation rate (m^2/s^3)	2.6	4.0

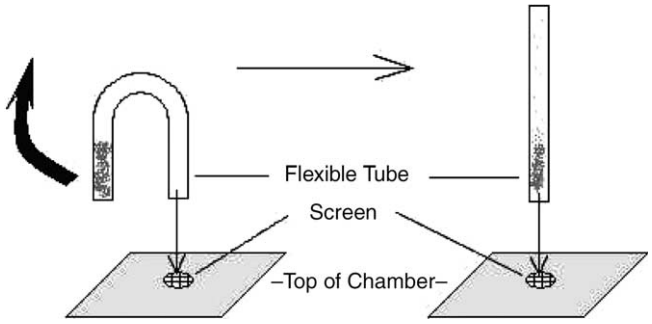

Fig. 2. Particle feed assembly.

resulting in a change in particle number density over time. The goal was to take images with a relatively fixed number of particles per image for each class of particles. Since the settling time of the particles varied, more trials were necessary to get the required number of images for the large glass particles, whereas fewer trials with more images per trial could be used for the slower settling lycopodium. While the number of particles suspended in turbulence remained relatively stable, the number of particles captured in each image varied roughly ±30% across all images.

Typically, approximately 5 g of lycopodium particles were introduced into the chamber resulting in a maximum possible particle-to-fluid mass loading ratio of 0.07, assuming the majority of the particles stayed suspended in the turbulence while images were taken. Approximately 18 g of glass particles were introduced, resulting in an estimated mass loading ratio of 0.023. This value was determined by measuring the mass loading from the images. This was necessary because the glass particles settled much faster, so the entire mass of introduced particles would be significantly higher than the actual mass of particles suspended. Due to this relatively small mass loading and the low Stokes number, turbulence modification by particles was expected to be small.

A Continuum Minilite dual-cavity Nd:YAG laser (25 mJ/pulse at 532 nm) was used to illuminate the falling particles. A series of lenses were placed to spread the laser beam into a vertical sheet passing through the center of the chamber. The laser sheet had a thickness of approximately 400 μm at the center of the image and increased to about 450 μm on the edges of the image. Images of the settling particles were taken with a Kodak ES1.0/10 CCD camera (10 bit, 1018×1008 pixels) placed perpendicular to the laser sheet, capturing a square domain of size 40 mm × 40 mm. The resulting images (Fig. 3a) were processed using LabVIEW IMAQ Vision software. The digital images were filtered using an appropriate threshold value to produce a binary image that distinguished between the particle and fluid phase. Next, a routine was performed to pick out and record the pixel coordinates of the center of each particle. Fig. 3(b) shows the uniquely identified particles as circles. The software was also able to distinguish between apparent overlapping particles. The resulting table of particle center coordinates was then used to analyze the particle concentration. Since the particles were nearly monodisperse, no attempt was made to measure the particle diameter.

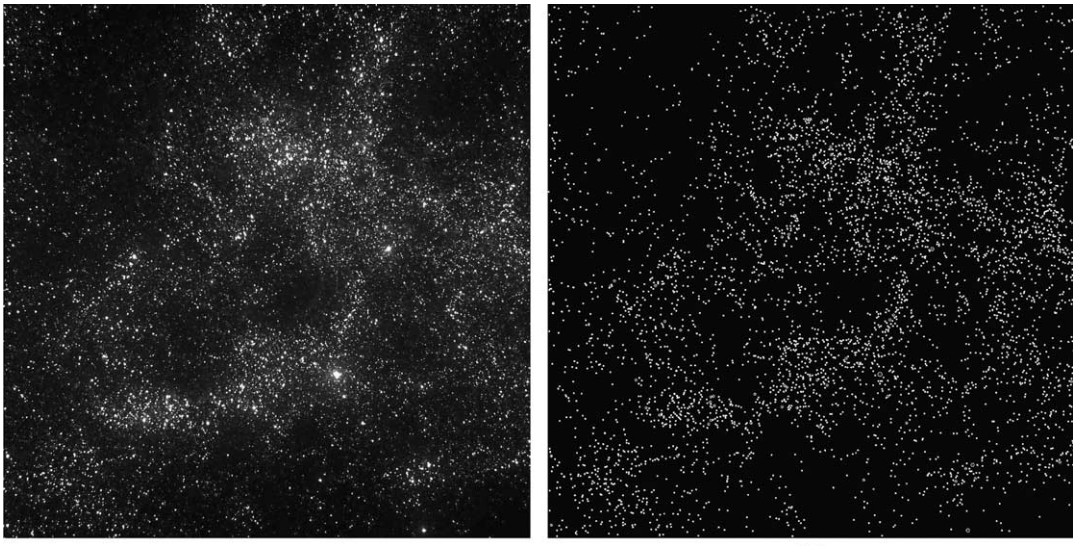

Fig. 3. (a) Original digital image; (b) positions of discrete particles picked out by software.

3. Results

One hundred and twenty five images were analyzed for each particle size and turbulence setting. The average number of particles per image was 1500, 3100, and 6400 for the 50 μm glass, 25 μm lycopodium, and 20 μm glass, respectively. Fig. 4 shows sample images from each particle class. From these images, it can be seen that particles with Kolmogorov Stokes numbers closer to one tend to group into clusters producing distinct regions of high and low particle concentrations, while particles with Stokes number near 10 produce a more uniform distribution. In an attempt to quantify the levels of preferential concentration, two techniques were used to analyze the particle concentration fields.

The first analysis of the particle position data followed the approach of Fessler et al. (1994). Each image was divided into a set of uniform size boxes, and the number of particles in each

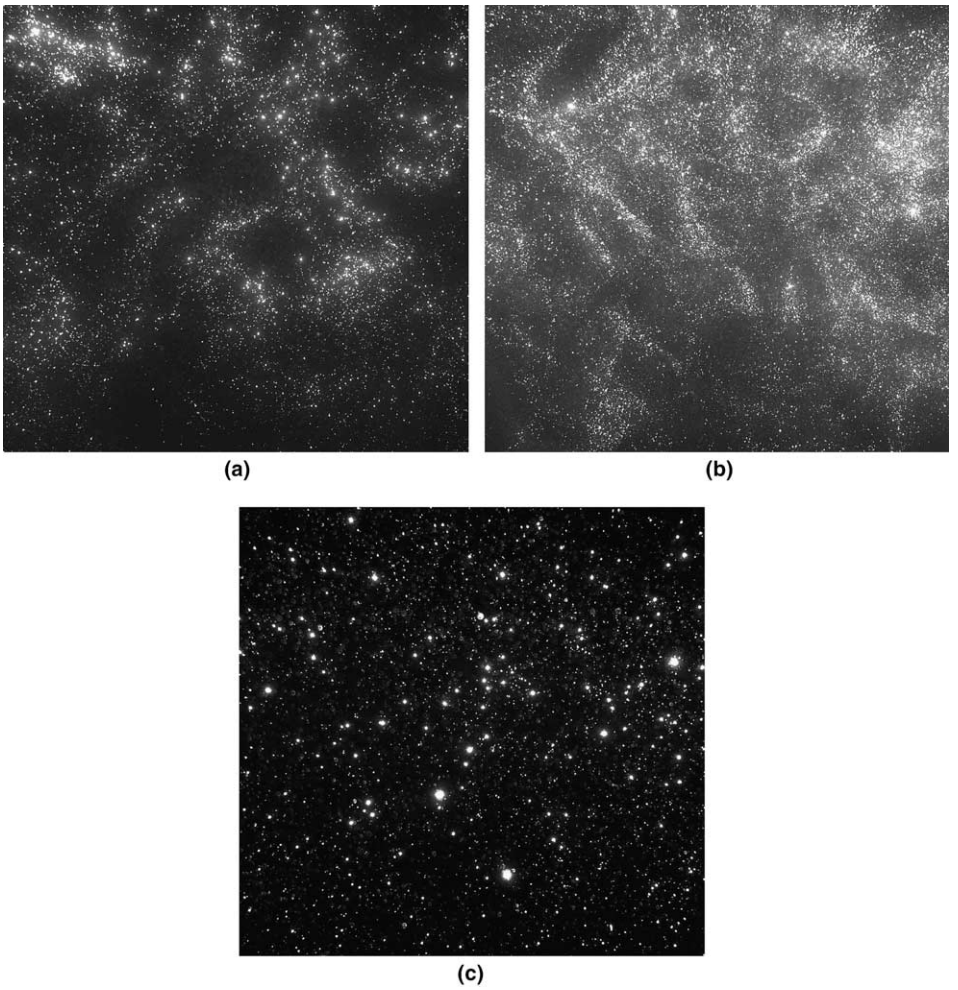

Fig. 4. Images of particles in homogeneous isotropic turbulence: (a) lycopodium, $St_k = 0.57$; (b) 20 μm glass, $St_k = 1.33$; (c) 50 μm glass, $St_k = 8.10$.

box was counted. For particles placed randomly in a field, the number of particles in each box should be distributed according to a Poisson distribution:

$$F(k) = (e^{-\lambda}\lambda^k)/k! \tag{3.1}$$

This Poisson distribution is characterized by two parameters: λ is the mean number of particles per box, and $F(k)$ is the probability that an integer number of particles, k, will be found in a given box. Following the idea of Fessler et al. (1994), the difference between the standard deviation of the measured distribution and the standard deviation of a random particle arrangement based on a Poisson distribution is a measure of preferential concentration. This parameter, D, is defined as

$$D = (\sigma - \sigma_p)/\lambda \tag{3.2}$$

where σ and σ_p correspond to the standard deviations for the experimental and Poisson distributions, respectively. This analysis was done over a range of grid sizes to determine the length scale of maximum preferential concentration.

Fig. 5(a) shows the experimental distribution and the corresponding Poisson distribution for the 20 μm diameter glass particles analyzed using 2 mm square boxes. The average number of particles per box is 22.5. It is apparent that boxes containing either no particles or a very large number of particles are much more probable for the experimental distribution than for a random distribution. The standard deviation of the experimental distribution is much larger, indicating strong preferential concentration. A similar comparison is made for the 50 μm diameter glass particles in Fig. 5(b), based on an average of 4.5 particles per 2 mm square box. For this case, the distribution of particles is much closer to the Poisson distribution, indicating a lesser degree of preferential concentration.

Values of the parameter D were averaged over all the images taken for a specific particle size and turbulence level, and compiled to produce the plot seen in Fig. 6. Here, the length of one side of the square grid, L, is normalized by the Kolmogorov length scale, η. As L increases towards infinity, D should approach zero, as Fig. 6 suggests for the smaller St_k particles. In our case, the image size prevents the deviation from being calculated at larger values of L. Different magnitudes of preferential concentration were observed, with the largest departure from a random concentration achieved with Stokes number nearest unity. The three curves with $St_k \sim 1$ were similar within experimental uncertainty. The same analysis was performed on a random distribution of 5000 simulated particles per image to validate the algorithm. It can be seen from the plot that particles placed randomly in the field give a D value near zero regardless of grid size. For both sets of glass particles, the turbulence levels were shifted by running the experiment at a different speaker setting, altering the Stokes number slightly. For these cases it can be seen that a shift towards a Stokes number of one results in a larger D value, indicating that preferential concentration occurs most strongly for Stokes number very near unity. Although the variation in Kolmogorov scale and Taylor microscale Reynolds number in the present experiment is small, the results corroborate conclusions from simulations performed at much lower Reynolds numbers. For comparison, two datasets from Fessler et al. (1994) are plotted against the experimental data. As can be seen, their dataset for Stokes number 19 has a lower peak value than that for our 50 μm glass particles with Stokes numbers 6 and 8, and maintains a comparable shape. Similarly, their dataset for Stokes number 2.2 follows the same trend as our near-unity datasets, and also has a lower peak value as expected. The data of Fessler et al. was taken at the centerline of a turbulent

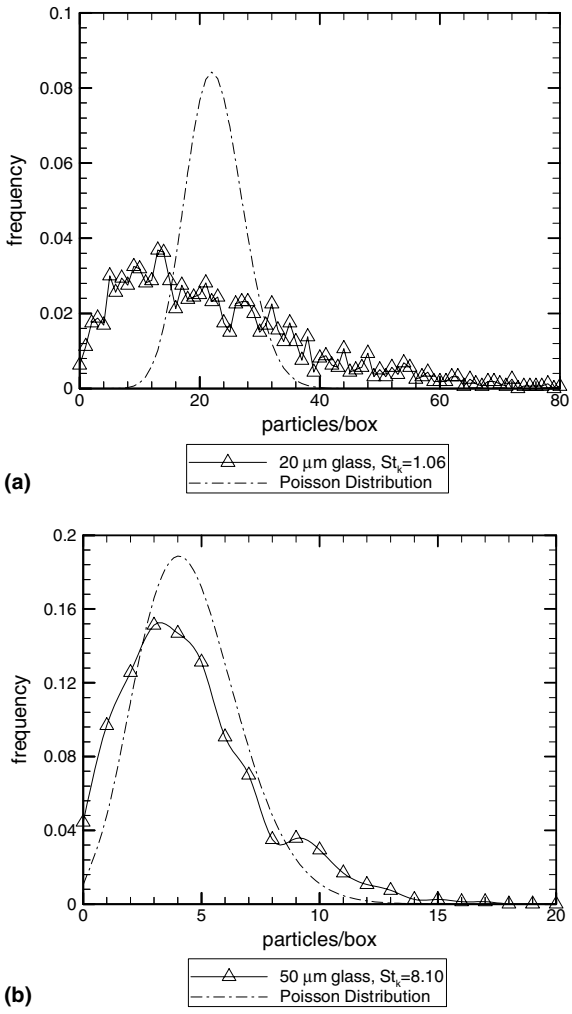

Fig. 5. Distribution of particle number density for (a) 20 μm glass; (b) 50 μm glass.

channel flow, where the turbulence was nearly homogeneous and isotropic. The turbulence was also generated at the walls, diffused inwards, and dissipated at the center, similar to our experiments.

A unique feature of the present work is the broader range of scales due to the higher Reynolds number as compared to the previous direct numerical simulation (DNS) studies. This provides a fairly broad range of scales over which preferential concentration occurs. For Stokes numbers near unity, there is a substantial peak in D for a box scale around 8–20 Kolmogorov length scales. The peak in D occurs at a much larger length scale for the higher Stokes number particles. These particles have little response to the smaller (shorter time scale) eddies, but are non-uniformly dispersed by the larger eddies in the flow.

Sundaram and Collins (1999) outlined the importance of the radial distribution function in determining the effect of preferential concentration on particle collisions. The radial distribution

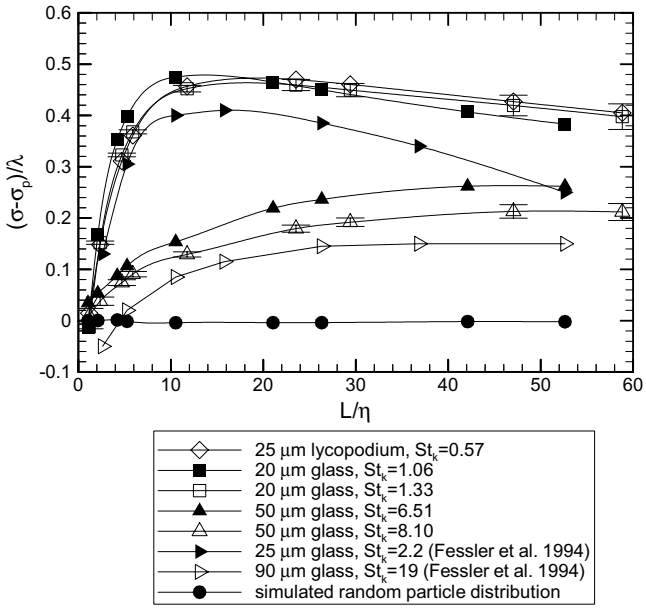

Fig. 6. Particle distribution deviation from random distribution (uncertainty results typical of all cases).

function (RDF) shows the relative density of particles in the space surrounding a particle as a function of distance from the particle. If particles are strongly preferentially concentrated, most particles will be located in regions of high concentration. Sundaram and Collins evaluated the RDF in spherical shells using DNS data. Using the present planar image data, we analyzed the RDF using annular domains.

In this process, a random particle was picked out of an image and a series of concentric circles were "drawn" around it, with radii increasing by steps of 0.2 mm, with the largest radius equal to 8 mm. Next, particles located between consecutive radii were counted to get an annular particle count. Approximately 25,000 test particles for each data set were examined, and the number of neighboring particles per annulus was averaged. The ratio of the average number of particles per annulus to the area of the annulus was calculated, giving the annular number density. This value was then normalized by the average number density over all 125 images, to obtain the RDF. The formula for the RDF is given in Eq. (3.3).

$$\mathrm{RDF} = \frac{N(r_i)A}{A(r_i)N} \tag{3.3}$$

where $N(r_i)$ and $A(r_i)$ represent the average number of particles and area within a particular annulus with radius r_i, respectively, N being the number of total particles averaged over all images, and A being the area per image. In this way, deviations from the average concentration are manifested as radial densities significantly higher or lower than one.

Fig. 7 shows the RDF for several experimental data sets as well as a set based on randomly placed particles, and data sets based on DNS data from Sundaram and Collins (1999). The RDF value is plotted against the normalized radius, r/η. As can be seen, the randomly distributed

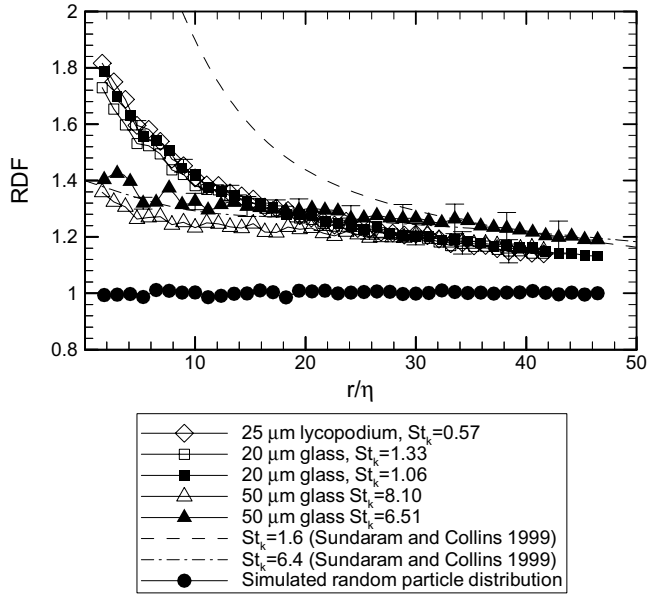

Fig. 7. Radial distribution function (uncertainty results typical of all cases).

particles quickly reach and stay at densities close to one, indicating a relatively uniform density. The particles with Kolmogorov Stokes numbers near one have significantly higher than average densities at small radii. The RDF of the case with Kolmogorov Stokes number near 10 shows a slightly elevated relative density around the same range of radii, but the magnitude of preferential concentration is considerably less, supporting the idea that preferential concentration occurs most dramatically at Stokes numbers near one. This experimental data matches well with the Sundaram and Collins data for Stokes number near 6, however the DNS results for Stokes number closer to 1 is relatively higher than the experimental results. This discrepancy may be attributed to differences between the three-dimensional domain used to obtain the DNS results, and the two-dimensional domain used experimentally. Due to the thickness of the laser sheet, RDF values for smaller annuli were deemed invalid, as the potential error caused by particles illuminated at different depths in the laser sheet is large at small radii. The uncertainty in this data was calculated based on the standard deviation in number of particles per annulus. As 200 particles were randomly selected from each image, and the largest annulus could not fit in the image 200 times without overlapping, not all of these samples were independent. Therefore, the uncertainty was determined using the maximum number of independent samples possibly taken based on annulus size.

4. Conclusions

An experimental study of the concentration of particles subjected to homogeneous and isotropic turbulence with no mean flow has been conducted. Digital images of three classes of particles at two different turbulence settings were obtained, analyzed, and compared to a simulated random

particle distribution. The deviation from a random concentration distribution for each data set was observed by two independent methods. Plots were made comparing the departure from a random distribution based on Stokes numbers obtained by using the Kolmogorov time scale. It was determined that the largest magnitude of preferential concentration occurs for Stokes numbers near unity for Taylor microscale Reynolds number near 230. This finding tends to validate the Kolmogorov time scale as the most appropriate fluid time scale for measuring preferential concentration, and also suggests that preferential concentration will be maximized at a Kolmogorov Stokes number near one for all Reynolds numbers. It was also observed that maximum preferential concentration occurs at a length scale on the order of 10η for particles with Stokes numbers near unity.

Acknowledgement

The research described in this paper was funded by NASA grant number NAG3-2738.

References

Fallon, T., Rogers, C.B., 2002. Turbulence-induced preferential concentration of solid particles in microgravity conditions. Exp. Fluids 33, 233–241.

Fessler, J.R., Kulick, K.D., Eaton, J.K., 1994. Preferential concentration of heavy particles in a turbulent channel flow. Phys. Fluids 6, 3742–3749.

Hogan, R.C., Cuzzi, J.N., 2001. Stokes and reynolds number dependence of preferential particle concentration in simulated three-dimensional turbulence. Phys. Fluids 13, 2938–2945.

Hwang, W., Eaton, J.K., 2004. Creating homogeneous and isotropic turbulence without a mean flow. Exp. Fluids 36, 444–454.

Maxey, M.R., 1987. The gravitational settling of aerosol particles in homogeneous and random flow fields. J. Fluid Mech. 174, 441–465.

Squires, K.D., Eaton, J.K., 1991. Preferential concentration of particles by turbulence. Phys. Fluids A 3, 1169–1178.

Sundaram, S., Collins, L.R., 1999. The modulation of isotropic turbulence by suspended particles. J. Fluid Mech. 379, 105–143.

Wang, L.P., Maxey, M.R., 1993. Settling velocity and concentration distribution of heavy particles in homogeneous isotropic turbulence. J. Fluid Mech. 256, 27–68.